NRIAG Journal of Astronomy and Geophysics 7 (2018) 214–219

Contents lists available at ScienceDirect

NRIAG Journal of Astronomy and Geophysics

journal homepage: www.elsevier.com/locate/nrjag

Full length article

Ionospheric scintillations detected by SCINDA-Helwan station during St. Patrick's Day geomagnetic storm

Ayman M. Mahrous[a], Makram Ibrahim[b], J. Berdermann[c], Hager M. Salah[a,d,*]

[a] Space Weather Monitoring Center, Faculty of Science, Helwan University, 11795 Cairo, Egypt
[b] National Research Institute of Astronomy and Geophysics (NRIAG), Helwan, 11421 Cairo, Egypt
[c] Institute of Communications and Navigation, German Aerospace Center, 17235 Neustrelitz, Germany
[d] Canadian International College in Cairo, 11835 Cairo, Egypt

ARTICLE INFO

Keywords:
GPS-SCINDA
Magnetic storm
Ionospheric scintillation
TEC (Total Electron Content)

ABSTRACT

We report about our observations during one of the major storms of the solar cycle, the so-called St. Patrick's Day storm, which happened on 17 March 2015. The St. Patrick's Day storm was the first storm of the current solar cycle that reached the level "Severe" on the NOAA geomagnetic storm scale. The CME arrived at the Earth about 04:30 UT on the 17th, the sudden storm commencement (SSC) was recorded at ~04:45 UT followed by a quick drop of the SYM-H index. The Kp planetary index of the geomagnetic activity had reached the maximum value of 8. The z-component of the interplanetary magnetic field (IMF) was strongly northward at the storm's day and altered to southward direction on the next day. The ionospheric response to that severe geomagnetic storm was detected using processed data from GPS-SCINDA receiver installed at Helwan station (Egypt; Geographic coordinates: 29.86°N, 31.32°E) with a dual frequency (f1 = 1.5 GHz, f2 = 1.2 GHz). Our results show that the Vertical Total Electron Content (VTEC) and the ionospheric scintillation index S4 reached the maximum value on the 17th. The ionospheric features during the storm are described within this study.

1. Introduction

A rapid fluctuation of amplitude and phase in radio signals can occur over the equatorial and low latitude region when passing through the ionosphere, this phenomenon is known as ionospheric scintillation and is based on the occurrence of plasma density irregularities in the ionosphere. The density irregularities are mostly indicators of the equatorial Spread-F (ESF) at altitudes ranging from 200 to 1000 km, with the primary disturbance region being between 250 and 400 km (Groves et al., 1997). By cause of the complex interaction between electric fields, the earth's magnetic field, and neutral winds, the ESF shows severe conditions within the F region of the ionosphere, extends to ± 20° of the magnetic equator (Sridharan et al., 2012). The existence of enhanced eastward electric fields and meridional neutral winds at night induce disturbance in the ionosphere producing plasma bubbles containing irregularities of different size (McClure et al., 1977), which cause scintillations in the passing radio signal through the ionosphere (Zou, 2011).

Particularly strong ionospheric irregularities were caused by the intense geomagnetic storm producing wave-like propagating structures known as large-scale traveling ionospheric disturbances (LSTIDs). They represent the manifestation of gravity waves created in the Auroral zones in the Northern and Southern Hemispheres. Such disturbances at the auroral oval can become a source of strong LSTIDs propagating toward the Equator (Hunsucker, 1982; Hajkowicz and Hunsucker, 1987). The most discussed source mechanisms for the excitation of LSTIDs are Joule heating, the Lorentz force (Oyama and Watkins, 2012) and also particle heating has to be considered. As long as the complexity of interactions between electric and magnetic fields together with the thermospheric winds, the exact generation mechanisms of LSTIDs are only poorly understood till now.

Several studies show that the ionospheric behavior during geomagnetic storms is changed from its normal behavior (Blagoveshchensky et al., 2003). The geomagnetic storm produces thermospheric winds, creates electric currents and changes the structure in the upper atmosphere. Every one of them can make a non-normal variation in the photoionization, recombination, and transport processes causing an irregular change in the electron concentration of the ionosphere. Some main effects are the significant change in the neutral wind circulation and atmospheric composition affecting the rate of production and loss of ionization. These changes modify and redistribute the atmospheric electron density. The neutral winds can also

Peer review under responsibility of National Research Institute of Astronomy and Geophysics.
* Corresponding author at: Space Weather Monitoring Center, Faculty of Science, Helwan University, 11795 Cairo, Egypt.
E-mail address: hager.m.salah.92@gmail.com (H.M. Salah).

https://doi.org/10.1016/j.nrjag.2018.05.007
Received 8 March 2017; Received in revised form 21 March 2018; Accepted 19 May 2018
Available online 25 May 2018
2090-9977/ © 2018 Published by Elsevier B.V. on behalf of National Research Institute of Astronomy and Geophysics This is an open access article under the CC BY-NC-ND license (http://creativecommons.org/licenses/BY-NC-ND/4.0/).

cause the production of F-region electric fields through the mechanism of disturbance dynamo. Such electric fields can also redistribute the F-region plasma, affecting the production and loss rates, and causes Total Electron Content (TEC) to change (Galav et al., 2011). The ionospheric scintillation is enhanced by these electron density variation (Shang et al., 2008).

All space-based communications, surveillance, broadcasting and reduce the accuracy of satellite based navigation and positioning as well as of augmentation systems used in precise aircraft landing procedures may have affected by Ionospheric variation. Ionospheric irregularities cause stresses to the tracking loop of Global Navigation Satellite System (GNSS) receiver (Skone et al., 2001).

The GPS signal at L-band frequencies is important for studying the features of ionospheric irregularities as it is affected by the irregularities of few hundred meters' scale sizes. Many researchers studied the GPS morphology based ionospheric scintillation in terms of S4 index at low latitude in different longitude regions. They found that the amplitude scintillation activity differs with magnetic activity, seasons, geographical location, local time and solar cycle (Tanna et al., 2013; Hlubek et al., 2014; Kriegel et al., 2017).

In the present paper, we investigate the behavior of VTEC and the ionospheric scintillation index S4 recorded at Helwan, Egypt (Geographic coordinates: 29.86°N, 31.32°E). The study is based on GPS-SCINDA data collected near the northern crest of the equatorial anomaly region during one of the major storms of the current solar cycle (solar cycle 24), which occurred on 17 March 2015. The so-called St. Patrick's Day storm emerged after double-halo coronal mass ejections (CMEs) that hit the Earth's magnetosphere at ~04:30 UT. This G4 storm is caused by two large eruptions left the Sun on 15 March 2015. These two Earth-directed CMEs added and accelerated together through the interplanetary space, resulting in the large geomagnetic storm with SYM-H index decreasing to its minimum of −223 nT.

2. Theory/calculations

The ionospheric contribution is proportional to the Total Electron Content, TEC, along the ray path between receiver and satellite. TEC is the total number of electrons in a column with one square meter cross-section area along the GPS signal path. It is measured in total electron content units (TECU; 1 TECU = 10^{16} electrons/m^2). Because of the dispersive nature of the ionosphere, the two radio signals of the GPS are delayed and their phases are advanced. Hence, the electron content along the GPS signal path between the satellite and receiver (STEC) can be obtained from (1) the difference between the pseudo ranges (P_1 and P_2), and from (2) the difference between the phases ($\varnothing_1$ and $\varnothing_2$) of the two signals via the following two equation respectively (Sardón et al., 1994):

$$STEC = \int_R^S N_e dr = \left[\frac{2}{K}\left(\frac{f_1^2 - f_2^2}{f_1^2 f_2^2}\right)\right](\Delta P_2 - \Delta P_1) \quad (1)$$

$$STEC = \int_R^S N_e dr = \left[\frac{2}{K}\left(\frac{f_1^2 - f_2^2}{f_1^2 f_2^2}\right)\right](\Delta \varnothing_2 - \Delta \varnothing_1) \quad (2)$$

where f_1 and f_2 are the frequencies of the two GPS radio signals.

It is necessary to calculate an equivalent vertical value of TEC (VTEC), which is independent of the elevation of the ray path and calculated by taking the projection from the slant to vertical using the thin shell model assuming a height of 350 km, given by (Klobuchar, 1986):

$$VTEC = STEC \times \cos\left[\arcsin\left(\frac{R_c \cos\theta}{R_c + h_{max}}\right)\right] \quad (3)$$

where $R_c = 6378$ km, $h_{max} = 350$ km, θ= elevation angle at the ground station.

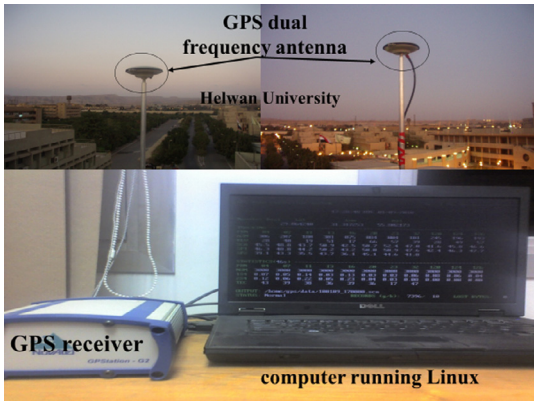

Fig. 1. SCINDA installation in Helwan University, Egypt.

The amplitude scintillation index, S4, is computed over 60-s intervals as the standard deviation of the received signal intensity (SI) normalized by its mean value and is referred to as the Total S4, which is computed as following (Gwal et al., 2006):

$$S_4(f) = \frac{\sqrt{\langle I\rangle^2 - \langle I\rangle^2}}{\langle I\rangle^2} \quad (4)$$

where I is signal intensity (amplitude squared), $\sqrt{\langle I\rangle^2 - \langle I\rangle^2}$ is the Signal intensity standard deviation and $\langle I\rangle$ is the Signal intensity mean.

3. Material and methods

The Scintillation Network and Decision Aid (GPS-SCINDA) dual UHF and L-band frequency receiver are installed at Helwan, Egypt located near the northern crest of the equatorial anomaly region, shown in Fig. 1. This system can track up to 11 GPS satellites at the L1 (1.57542 GHz) and L2 (1.2276 GHz) frequency simultaneously. The GPS-SCINDA system consists of a GPS antenna, a GPS receiver, the GPS -SCINDA data collection software and a computer running LINUX with access to the Internet. The SCINDA software records data streams from the receiver and computes post-processed parameters such as scintillation intensity (S4) index and TEC. In addition, information about the tracked satellite are shown on the computer screen. In this study, only the measurements for satellite elevation angles above 30° are taken into account in order to reduce the multipath effect on the observation. We analyze theses data to study the ionospheric response to the St. Patrick's Day storm and the occurrence of scintillation at Helwan station.

4. Results and discussion

A CME reached the Earth on March 17th 2015 around 04:30 UT causing a geomagnetic storm as shown in Fig. 2(a–f) which lasts from 16th till 21st of March 2015. The solar wind speed Vx, Auroral Electrojet AE, AU-AL indices, the Interplanetary Magnetic Field with a southward Bz and Earth's magnetosphere (IMF-Bz), the global geomagnetic storm Kp index, and the symmetric disturbance field in H direction SYM-H component of the magnetic field are presented from the top to the bottom panel, respectively, as a function of the universal time throughout the corresponding period. The vertical red line indicates the storm onset time at 04:45 UT. Fig. 2 reveals that there was a sharp increase from about 13 nT to 25 nT of the SYM-H index at about 04:45 UT on 17 March indicating the CME arrival and sudden storm commencement (SSC) followed by an increase up to 56 nT at about 06:00 UT. At about 10:00 UT, the SYM-H began to decrease to −73 nT as the storm started to intensify. The storm conditions persisted for most of the day with some brief recoveries before the storm attained its minimum SYM-H value of −222 nT around 23:00 UT. The storm recovered to pre-storm conditions on March 18th. There was a distinct

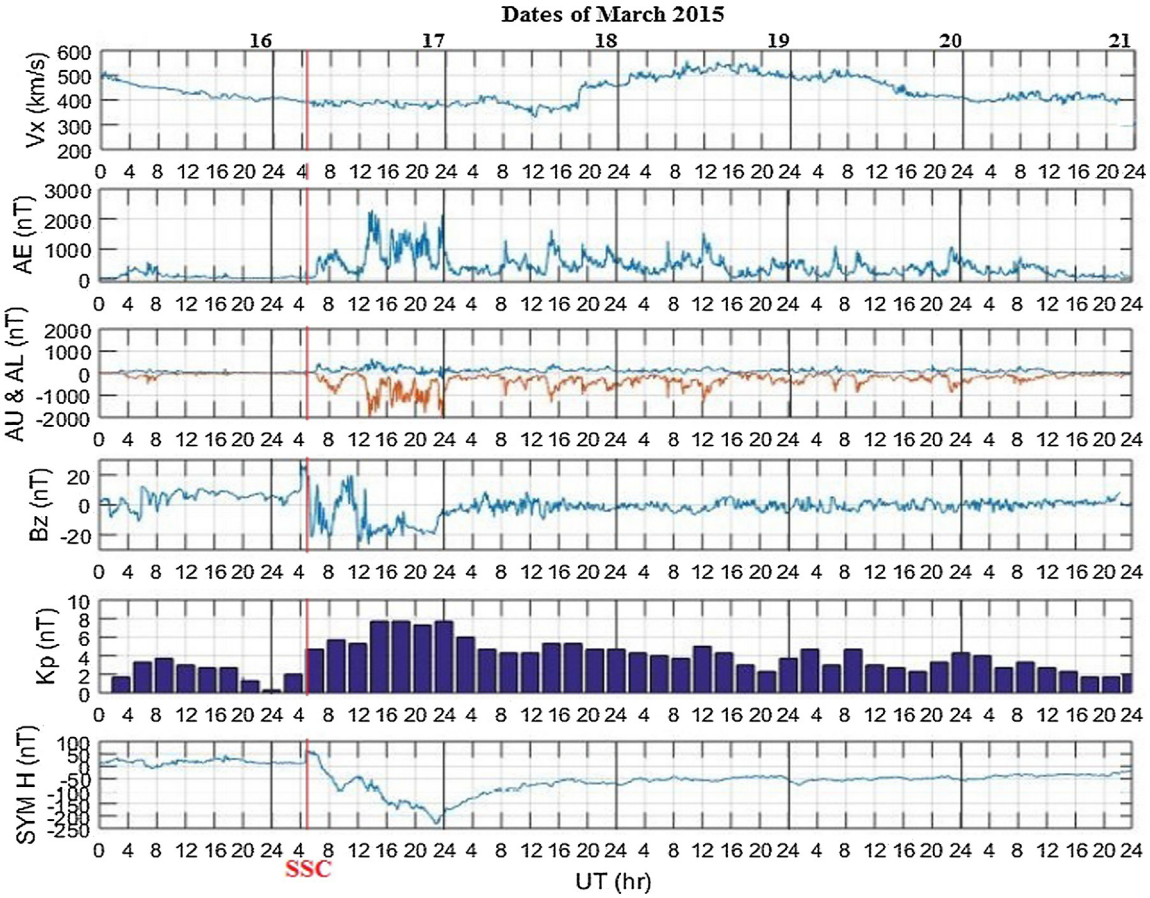

Fig. 2. The solar wind parameters and geomagnetic indices for St. Patrick's Day Storm, from top to bottom: (a) Vx component of the solar wind speed in km/s, (b) Auroral Electrojet index (values each min), (c) AU-AL indices (values each min), (d) the Bz component of the interplanetary magnetic field (at four min intervals), (e) Kp index (three-hourly), (f) SYM-H component of magnetic field (one min values), shown versus UT. The red line indicates the storm onset at 04:45 UT. (For interpretation of the references to colour in this figure legend, the reader is referred to the web version of this article.)

response to the solar wind parameters at the time of the SSC. The velocity of the solar wind increased from about 420.3 to 599.3 km/s and the Auroral Electrojet (AE) index was about 2000 nT after 12 UT. The z-component of the interplanetary magnetic field (IMF) had a strong northward direction at the first but changed sharply to a southward orientation decreasing till −20 nT and remained predominately southward with some northward fluctuations. The Kp planetary index of the geomagnetic activity reached magnitude 5 and increased further to its maximum value of 8 after 12:00 UT.

For more clarification about the behavior of the storm, we plot the SYM-H index in Fig. 3 during the storm day on 17 March 2015 only. We observed the effect of the shock wave associated with a cloud of plasma ejected by the CME, as detected by the sudden storm commencement (SSC), is indicated by a vertical red line. This shock was accompanying to an increase in the magnetic SYM-H index (+13 nT to +56 nT). The compression phase continued from 04:45UT to 06:20 UT. At the end of the compression phase, the SYM-H decreased and reached the minimum value of −73 nT around 10:00 UT. From 09:30 UT until 12:00 the SYM-H increased from −73 nT to −44 nT. It is a partial recovery phase. Then, the SYM-H slowly decreased from 12:00 UT to 24:00 UT, as an effect of a second CME happened, and it reached its minimum value −222 nT before midnight. This was the end of the main phase of the storm that continued 18 hr.

In Fig. 4 the temporal change of the vertical Total Electron Content (TEC) is shown, which gives direct insight about the ionospheric perturbations over Helwan induced by the St. Patrick's Day storm (blue line). The mean value of the most quiet days of the month was taken as a reference (red line), where the dominant contribution to the diurnal variation in TEC is due to ionization from solar radiation. Again, the red vertical line indicates the SSC. According to the published results from WDC-Kyoto website, we chose the five international quietest days of 10, 30, 5, 14, and 9 in March 2015, and calculate the mean for the TEC data of those five days. The results show that during the storm day the vertical TEC initially shows quite normal behavior even past the SSC until 9:00 UT, followed by a sudden increase with two maxima at about 11:00 and 18:00. This increase is most dominant at 11:00 UT with mean TEC values up to 72.2 TEC units (red arrow) showing a large deviation to quiet ionospheric conditions. The vertical TEC at 18:00 increased again to 51 TEC units while the mean vertical TEC value was 37.5, this second enhancement is believed to be caused by the pre-reversal enhancement effect.

Fig. 5 represents the hourly variation of Delta TEC over Helwan induced by Patrick's Day storm. We observe a TEC enhancement (positive storm effect) post the SSC and during the partial recovery phase of the storm on 17 March 2015. At 09:30 UT, the positive storm effect is 7.5% of the $vTEC_{quiet}$. At 11:00 UT, the positive storm effect is 106% of the $vTEC_{quiet}$. Negative storm effect, i.e. ionization depletions, occurred after the enhancements. Transient TEC depletions with a maximum depletion of 84% of the $vTEC_{quiet}$ occurred during the main phase at 14:30 UT.

The 3-d surface plot of the scintillation index showing the variability of S4 values during March 2015 with a notable peak during the storm time, Fig. 6.

Fig. 7 shows the diurnal variation of L-band scintillation as represented by S4 index over Helwan station as obtained using GPS SCINDA receiver for the day 17th March 2015. The observations show

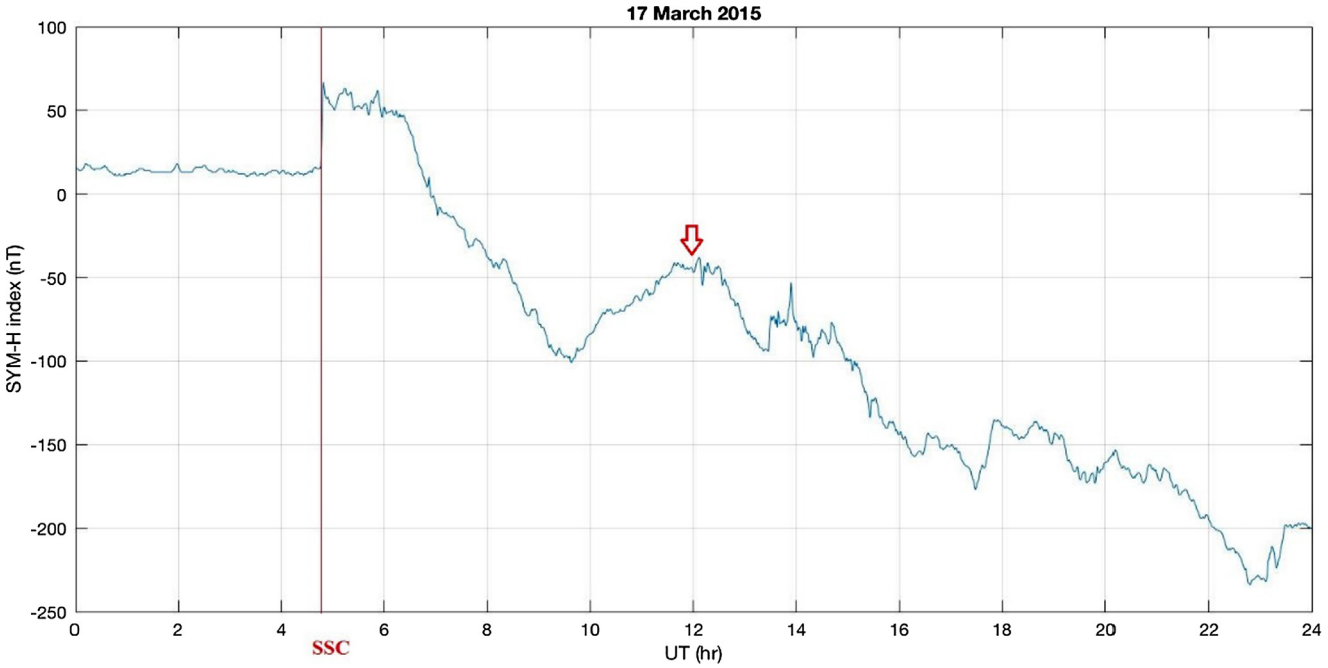

Fig. 3. SYM-H component of magnetic field (one min values), shown versus UT during the storm day on 17 March 2015. The red line indicates the storm onset at 04:45 UT. (For interpretation of the references to colour in this figure legend, the reader is referred to the web version of this article.)

GPS ionospheric scintillation started occurring at 12:00 UT and continued until 14:00 UT with S4 index reaching 0.16 at 12:03 UT suggesting disturbed scintillation behavior on this day. The scintillation enhancement immerged corresponding to the local minimum SYM-H value of −44 nT (showed by the red arrow in the bottom panel in Fig. 3), enhancement in VTEC, and enhancement in delta TEC values (positive storm effect). It is worthwhile to note that the triggered scintillation probably associated with the local minimum SYM-H determined time.

Whether a magnetic storm triggering/inhibiting ionospheric scintillation or not is still a disputed topic. The debates mostly focused on the dominated factor in the triggering inhibition effects during the storm. The results of (Borries et al., 2016) showed that, the storm on 17 March 2015 in the European-African sector produced a large-scale traveling ionospheric disturbances (LSTID) at the beginning of the partial recovery phase at 10:30 UT, propagating toward the equator from 60°N reaching 28°N at 12:15 UT. The LSTID had very large wave parameters (wavelength: ≈3600 km, speed: ≈500 m/s, and period: ≈120 min). The results of Borries et al. (2016) estimates an arrival time of the LSTIDs at Helwan station, at about 11:00 UT indicated in Fig. 4 by the red arrow. Thus, the weak features of a possible scintillation event may be explained by the fact that a strong ionospheric perturbation was engendered by Patrick's day intense storm producing LSTID, and we observed its signature over Helwan, Egypt resulting in a VTEC enhancement, positive storm effect, may producing weak scintillation activities.

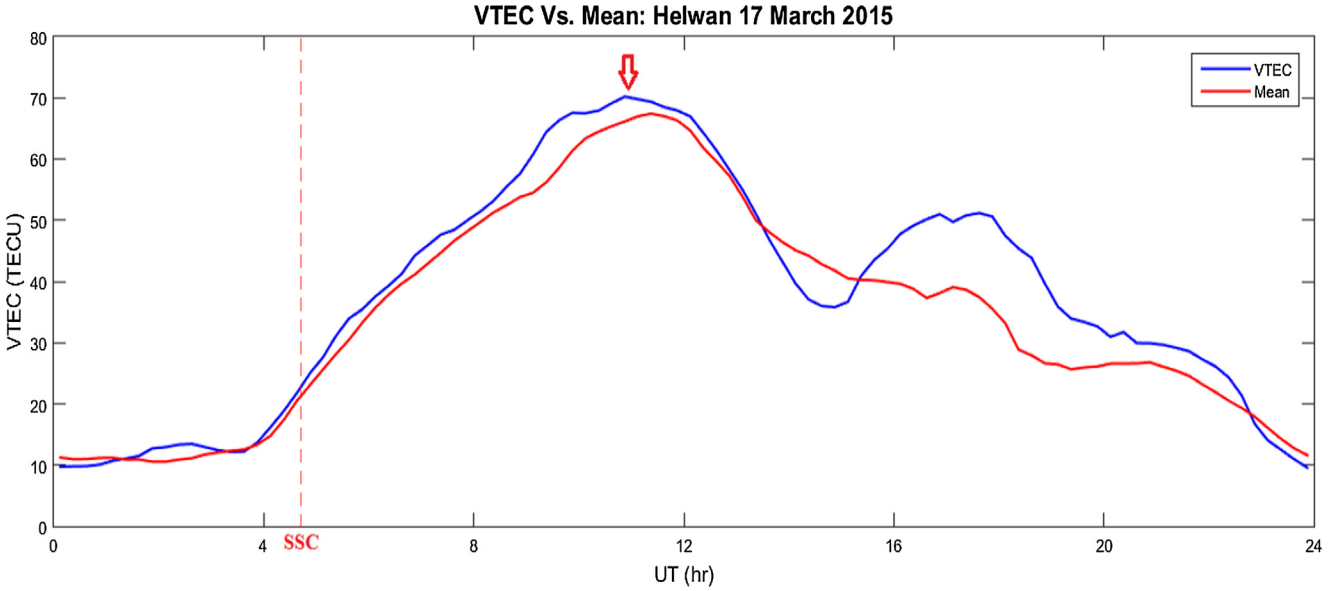

Fig. 4. Comparison between the diurnal variation of VTEC at SCINDA-Helwan station (the blue line) and the mean of the referenced quiet days (the red line), during the St. Patrick's Day Storm (March 17th, 2015), the red vertical line indicates the SSC. (For interpretation of the references to colour in this figure legend, the reader is referred to the web version of this article.)

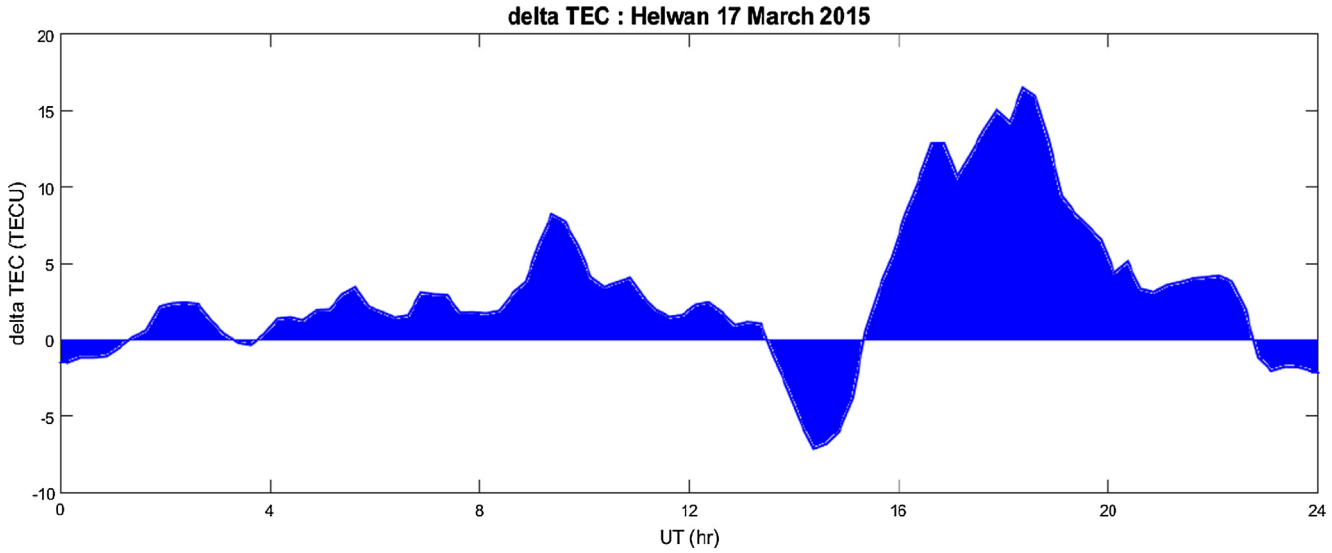

Fig. 5. Hourly variation of Delta vertical TEC over Scindia- Helwan station during the St. Patrick's Day storm.

5. Conclusion

The present paper reports about the features of VTEC and L-band ionospheric scintillation S4 during the St. Patrick's Day sever geomagnetic storm on 17 March 2015 recorded by the GPS-SCINDA receiver at Helwan low latitude station located near the northern crest of the equatorial anomaly region.

The study shows that:

1. A sudden increase in VTEC values at 09:30 UT occurred after the SSC with a positive storm effect of 2.3% of the vTECquiet. The super storm seems to the enhancement of ionospheric electron density.
2. A weak scintillation enhancement reaching 0.16 at 11:30 UT, is associated with the local minimum SYM-H value of −63 nT, abrupt enhancement in VTEC, and positive storm effect of 127.6% of the $vTEC_{quiet}$. The observations suggest that this feature of this scintillation event may be explained by the fact that a strong ionospheric perturbation was engendered by Patrick's day intense storm producing LSTID.
3. The vertical TEC also increased at 14:45 UT with a negative ionospheric storm with a maximum depletion of 94.3% of the $vTEC_{quiet}$. This enhancement is believed to be caused by the Pre-reversal enhancement effect.

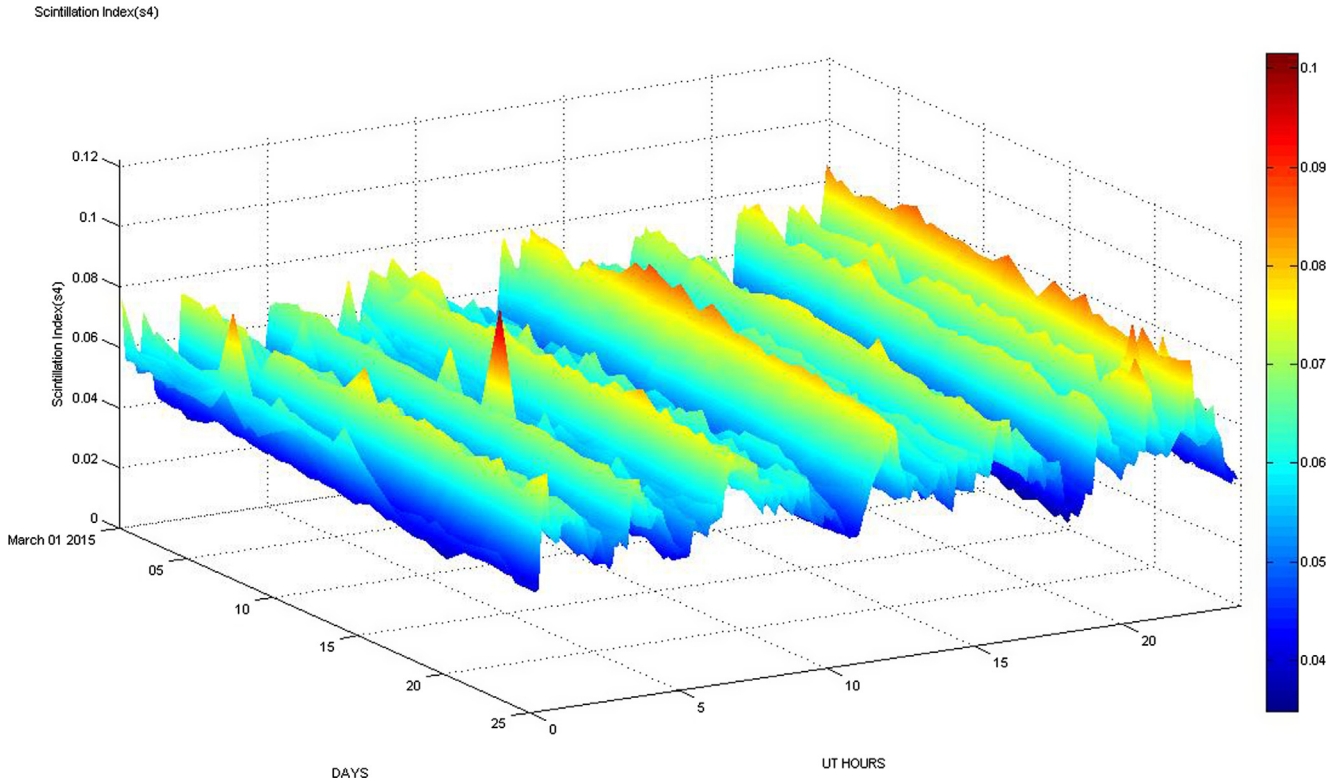

Fig. 6. 3D- surface plot for the scintillation index S4 during March 2015, showing the effects of the Patrick's Day Storm (March 17th, 2015) on the signal scintillation.

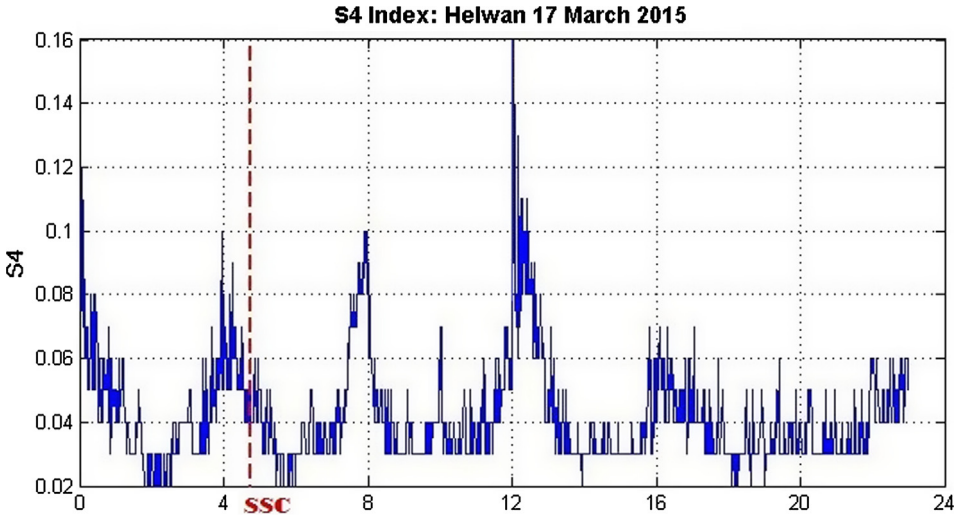

Fig. 7. The diurnal variation of the scintillation index S4 at SCINDA-Helwan station, during the Patrick's Day Storm (March 17th, 2015).

Acknowledgments

The authors are grateful to the Data Analysis Center for Geomagnetism and Space Magnetism, Graduate School of Science, Kyoto University for providing the geomagnetic data used in this research by website: (http://wdc.kugi.kyoto-u.ac.jp/), the website: (http://www.spaceweather.com) for making available the description of the solar event, and SCINDA-Helwan Station for providing access to the real-time display of satellite tracking status and the ionospheric parameters.

References

Blagoveshchensky, D.V., Pirog, O.M., Polekh, N.M., Chistyakova, L.V., 2003. Mid-latitude effects of the May 15, 1997 magnetic storm. J. Atmospheric Sol.-Terr Phys. 65, 203–210. http://dx.doi.org/10.1016/S1364-6826(02)00227-4.

Borries, C., Mahrous, A.M., Ellahouny, N.M., Badeke, R., 2016. Multiple ionospheric perturbations during the Saint Patrick's Day storm 2015 in the European-African sector. J. Geophys. Res. Space Phys. 121http://dx.doi.org/10.1002/2016JA023178. 2016JA023178.

Galav, P., Sharma, S., Pandey, R., 2011. Study of simultaneous penetration of electric fields and variation of total electron content in the day and night sectors during the geomagnetic storm of 23 May 2002. J. Geophys. Res. Space Phys. 116, A12324. http://dx.doi.org/10.1029/2011JA017002.

Groves, K.M., Basu, S., Weber, E.J., Smitham, M., Kuenzler, H., Valladares, C.E., Sheehan, R., MacKenzie, E., Secan, J.A., Ning, P., McNeill, W.J., Moonan, D.W., Kendra, M.J., 1997. Equatorial scintillation and systems support. Radio Sci. 32, 2047–2064. http://dx.doi.org/10.1029/97RS00836.

Gwal, A., Dubey, S., Wahi, R., Feliziani, A., 2006. Amplitude and phase scintillation study at Chiang Rai, Thailand. Adv. Space Res. 38, 2361–2365. http://dx.doi.org/10.1016/j.asr.2006.02.057. (Middle and Upper Atmospheres, Active Experiments, and Dusty Plasmas).

Hajkowicz, L.A., Hunsucker, R.D., 1987. A simultaneous observation of large-scale periodic TIDs in both hemispheres following an onset of auroral disturbances. Planet. Space Sci. 35, 785–791. http://dx.doi.org/10.1016/0032-0633(87)90038-9.

Hlubek, N., Berdermann, J., Wilken, V., Gewies, S., Jakowski, N., Wassaie, M., Damtie, B., 2014. Scintillations of the GPS, GLONASS, and Galileo signals at equatorial latitude. J. Space Weather Space Clim. 4, A22. http://dx.doi.org/10.1051/swsc/2014020.

Hunsucker, R.D., 1982. Atmospheric gravity waves generated in the high-latitude ionosphere: a review. Rev. Geophys. 20, 293–315. http://dx.doi.org/10.1029/RG020i002p00293.

Klobuchar, J.A., 1986. Design and characteristics of the GPS ionospheric time delay algorithm for single frequency users. In: Presented at the PLANS '86 - Position Location and Navigation Symposium, pp. 280–286.

Kriegel, M., Jakowski, N., Berdermann, J., Sato, H., Mersha, M.W., 2017. Scintillation measurements at Bahir Dar during the high solar activity phase of solar cycle 24. Ann. Geophys. 35, 97–106. http://dx.doi.org/10.5194/angeo-35-97-2017.

McClure, J.P., Hanson, W.B., Hoffman, J.H., 1977. Plasma bubbles and irregularities in the equatorial ionosphere. J. Geophys. Res. 82, 2650–2656. http://dx.doi.org/10.1029/JA082i019p02650.

Oyama, S., Watkins, B.J., 2012. Generation of atmospheric gravity waves in the polar thermosphere in response to auroral activity. Space Sci. Rev. 168, 463–473. http://dx.doi.org/10.1007/s11214-011-9847-z.

Sardón, E., Rius, A., Zarraoa, N., 1994. Estimation of the transmitter and receiver differential biases and the ionospheric total electron content from Global Positioning System observations. Radio Sci. 29, 577–586. http://dx.doi.org/10.1029/94RS00449.

Shang, S.P., Shi, J.K., Kintner, P.M., Zhen, W.M., Luo, X.G., Wu, S.Z., Wang, G.J., 2008. Response of Hainan GPS ionospheric scintillations to the different strong magnetic storm conditions. Adv. Space Res. 41, 579–586. http://dx.doi.org/10.1016/j.asr.2007.05.020.

Skone, S., Knudsen, K., de Jong, M., 2001. Limitations in GPS receiver tracking performance under ionospheric scintillation conditions. Phys. Chem. Earth Part Solid Earth Geod. 26, 613–621. http://dx.doi.org/10.1016/S1464-1895(01)00110-7. (Proceedings of the First COST Action 716 Workshop Towards Operational GPS Meteorology and the Second Network Workshop of the International GPS Service (IGS)).

Sridharan, R., Bagiya, M.S., Sunda, S., 2012. A novel method based on GPS TEC to forecast L band scintillations over the equatorial region through a case study. J. Atmosp. Sol.-Terr. Phys. 80, 230–238. http://dx.doi.org/10.1016/j.jastp.2012.02.007.

Tanna, H.J., Karia, S.P., Pathak, K.N., 2013. A study of L band scintillations during the initial phase of rising solar activity at an Indian low latitude station. Adv. Space Res. 52, 412–421. http://dx.doi.org/10.1016/j.asr.2013.03.022.

Zou, Y., 2011. Ionospheric scintillations at Guilin detected by GPS ground-based and radio occultation observations. Adv. Space Res. 47, 945–965. http://dx.doi.org/10.1016/j.asr.2010.11.016.